Supporting Information

Diamondoid-Structured Polymolybdate-Based Metal-Organic Frameworks as High-Capacity Anodes for Lithium-Ion Batteries

Yuan-Yuan Wang,[a‡] Mi Zhang,[b‡] Shun-Li Li,[b] Shu-Ran Zhang,[a] Wei Xie,[a] Jun-Sheng Qin,[a] Zhong-Min Su*[a] and Ya-Qian Lan*[a,b]

[a]Institute of Functional Material Chemistry, Department of Chemistry, National & Local United Engineering Lab for Power Battery, Northeast Normal University, Changchun 130024, P. R. China

[b]Jiangsu Key Laboratory of Biofunctional Materials, School of Chemistry and Materials Science, Nanjing Normal University, Nanjing 210023, P. R. China

‡ These authors contributed to this work equally.

Corresponding Author: zmsu@nenu.edu.cn; yqlan@njnu.edu.cn.

S1. Materials and measurements

All the chemicals were obtained from commercial ources and were used without further purification. The FT-IR spectra were recorded from KBr pellets in the range 4000-400 cm^{-1} on a Mattson Alpha-Centauri spectrometer. Elemental analyses (C, N, and H) were measured on a Perkin-Elmer 2400 CHN elemental analyzer; P, Mo and Zn were determined with an inductively coupled plasma atomic emission spectrometer (ICP-AES). Thermogravimetry was carried out under nitrogen with a Perkin-Elmer TG-7 analyzer heated from room temperature to 700 °C at a ramp rate 5 °C min^{-1}. PXRD measurements were recorded ranging from 3 to 50° at room temperature on a Bruker D8 Advance diffractometer with Cu Kα (λ = 1.5418 Å). Electrochemical impedance spectroscopy (EIS) measurements and cyclic voltammetry (CV) were conducted on CHI 660D (Shanghai, China) electrochemical workstation at room temperature. Morphology analysis was conducted on a scanning electron microscope (SEM, JSM-7600F) at an acceleration voltage of 10 kV.

Electrochemistry

The sample and super P carbon were ground together by hand and then mixed with the polyvinylidene fluoride (PVDF) binder in N-methyl-2-pyrrolidinone (NMP) solvent to form slurry. The final mixture consisted 50% active material, 40% super P carbon and 10% PVDF binder. The slurry was deposited onto copper foils and dried under a vacuum at 60 °C for 24 h. The mass of each electrode was approximately 1 mg. Coin type cells were assembled in a glove box under Ar atmosphere, with oxygen and water concentration was maintained below 1 ppm, where the lithium metal anode was separated by a Whatman glass fiber membrane. 1 M $LiPF_6$ dissolved in a mixture of ethylene carbonate (EC) and diethyl carbonate (DEC) (1:1 v/v) was served as electrolyte. Before electrochemical tests, the batteries were soaked overnight.

S2. Single-crystal X-ray diffraction

Single-crystal X-ray diffraction data for **NENU-506** and **NENU-507** was recorded by using a Bruker Apex CCD diffractometer with graphite-monochromated Mo-Kα radiation (λ = 0.71069 Å) at 293 K. Absorption corrections were applied by using a multi-scan technique. The structure was solved by Direct Method of SHELXS-97 and refined by full-matrix least-squares techniques using the SHELXL-97 program within WINGX. Those hydrogen atoms attached to lattice water molecules were not located. For **NENU-506** and **NENU-507**, the data were corrected with SQUEEZE, a part of the PLATON package of crystallographic software used to calculate the solvent molecules or counterions disorder area and to remove the contribution to the overall intensity data. The detailed crystallographic data and structure refinement parameters for **NENU-506** and **NENU-507** are summarized in Table S1.

S3. Synthesis of NENU-506 and NENU-507

Hydrothermal synthesis was carried out in a 15 mL Teflon-lined stainless steel container under autogenous pressure. All reactants were stirred briefly before heating. The products were isolated by filtration and washed with ethanol. **NENU-506** was prepared from a mixture of sodium molybdate dihydrate (0.618 g, 2.55 mmol), Mo powder 99.99% (0.050 g, 0.52 mmol), H_3PO_3 (0.020 g, 0.25 mmol), zinc chloride (0.136 mg, 1 mmol), isonicotinic acid (0.120 g, 1 mmol), 40 wt % tetrabutylammonium hydroxide solution in water (120 μL, 0.18 mmol) and H_2O (6 mL). The pH was adjusted to 4.8 with 2 M HCl. The mixture was heated to 180 °C in 1 h, and the temperature was maintained for 72 h. After cooling to room temperature at 10 °C·h^{-1}, dark-red crystals suitable for XRD study were harvested. The crystals were obtained in a 64% yield based on IN. Elemental microanalysis for $C_{60}H_{118}Mo_{12}N_5O_{44}PZn_4$: C, 23.57; H, 3.89; Mo, 37.66; N, 2.30; P, 1.01; Zn, 8.55. Found: C, 22.66; H, 3.80; Mo, 37.50; N, 2.39; P, 1.02; Zn, 8.26. IR (Fig. S2, KBr pellets, ν/cm^{-1}): 3446 (w), 2960 (w), 2872 (w), 1556 (w), 1375 (m), 1215 (w), 940 (s), 907 (m), 812 (s), 779 (s), 694 (m), 647 (m), 595 (s), 549 (m), 480 (m). **NENU-507** was isolated by an analogous method with **NENU-506**, only using 4-(pyridin-4-yl) benzoic acid (HPBA) (0.200 g, 1 mmol) in substitution for isonicotinic acid. Elemental microanalysis for $C_{72}H_{124}Mo_{12}N_5O_{45}PZn_4$: C, 26.83; H, 3.88; Mo, 35.72; N, 2.17; P, 0.96; Zn, 8.11. Found: C, 25.56; H, 3.91; Mo, 35.97; N, 1.29; P, 0.96; Zn, 8.08. IR (Fig. S2, KBr pellets, ν/cm^{-1}): 3445 (w), 2961 (m), 2872 (m), 1559 (m), 1470 (m), 1350 (s), 1148 (w), 942 (s), 819 (s), 777 (s), 707 (m), 590 (m), 486 (w).

S4. Calculation of the theoretical capacities

The theoretical capacities were calculated according to equation (1):

$$Q = \frac{nF}{3.6M} = \frac{96500n}{3.6M} \qquad (1)$$

Q: Reversible charging-discharging capacity; n: Number of electrons; M: Molecular weight.

Owing to the intercalation mechanism for Li storage (equations 2-4), we consider the redox reactions of metal ions (Mo and Zn), which is also confirmed by the XPS results in Supplementary Fig. S17.

$$Mo^{6+} \leftrightarrow Mo^{4+} \qquad (2)$$

$$Mo^{5+} \leftrightarrow Mo^{4+} \qquad (3)$$

$$Zn^{2+} \leftrightarrow Zn \qquad (4)$$

If eight Mo (V), four Mo (VI) and four Zn (Ⅱ) ions in **NENU-507** are reduced to Mo^{4+} and metallic zinc, respectively, and possible lithiation/delithiation sites for coordination with Li in the organic ligands, maximum of n = 28, Q_{POMOF} = 233 mA h g^{-1}

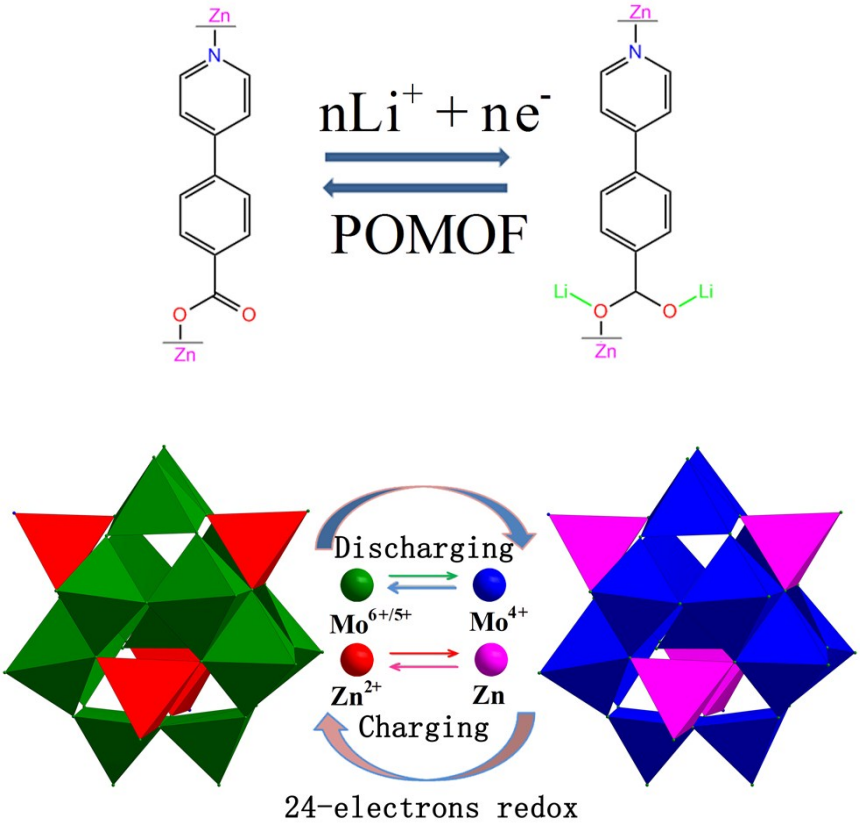

Scheme S1 The schematic diagram of the possible mechanism for the capacity of **NENU-507.**

Table S1. Crystal data and structure refinements for two compounds

	NENU-506	NENU-507
Empirical formula	$C_{60}H_{118}Mo_{12}N_5O_{44}PZn_4$	$C_{72}H_{124}Mo_{12}N_5O_{45}PZn_4$
Formula weight	3057.33	3223.49
Crystal system	Orthorhombic	Tetragonal
Space group	*Pbcn*	$I4_1/acd$
***a* (Å)**	25.686(5)	29.4436(11)
***b* (Å)**	31.770(5)	29.4436(11)
c (Å)	25.129(5)	54.543(4)
***α* (°)**	90.000(5)	90.00
***β* (°)**	90.000(5)	90.00
***γ* (°)**	90.000(5)	90.00
***V* (Å^3)**	20506(7)	47285(4)
Z	4	16
D_{calc}**(Mg·m^{-3})**	1.981	1.811
Abs.coeff.(mm^{-1})	2.424	2.109
***F*(000)**	12032	25440.0
Reflns collected	100966/18074	171919/14862
GOFon F^2	0.998	1.059
R_{int}	0.0961	0.1283
R_1[a]	0.0832	0.0750
wR_2**(all data)**[b]	0.2245	0.2348

[a] $R_1=\Sigma||F_o|-|F_c||/\Sigma|F_o|$. [b] $wR_2=|\Sigma w(|F_o|^2-|F_c|^2)|/\Sigma|w(F_o^2)^2|^{1/2}$

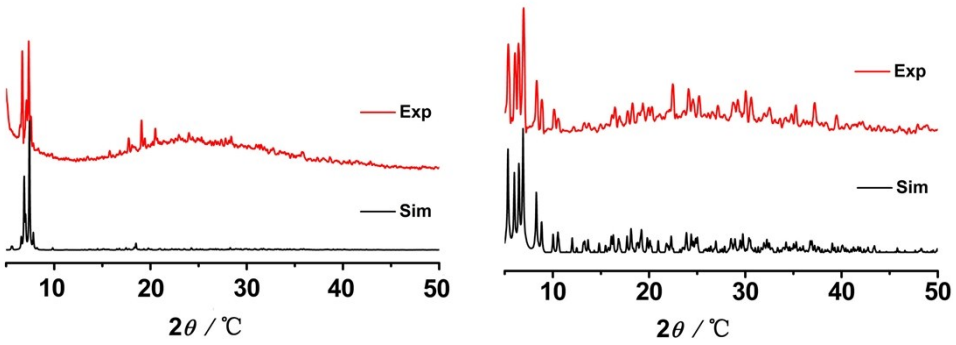

Fig. S1 X-Ray powder diffraction patterns of **NENU-506** (*left*) and **NENU-507** (*right*): as-synthesized (red) and simulated (black).

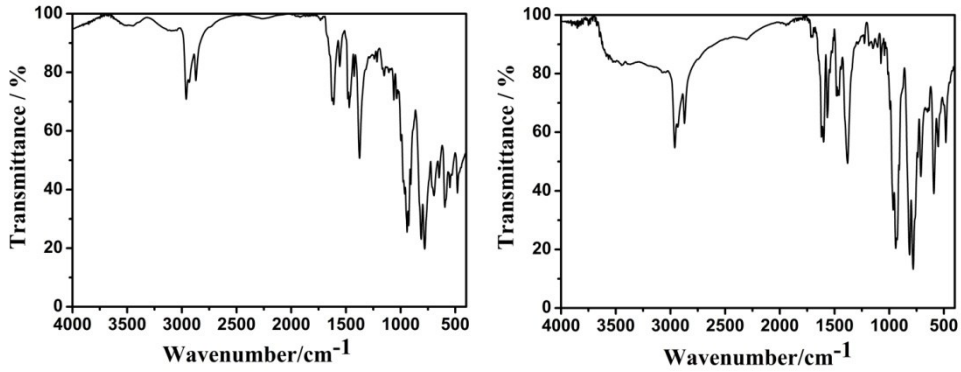

Fig. S2 The IR spectra of **NENU-506** (*left*) and **NENU-507** (*right*), respectively.

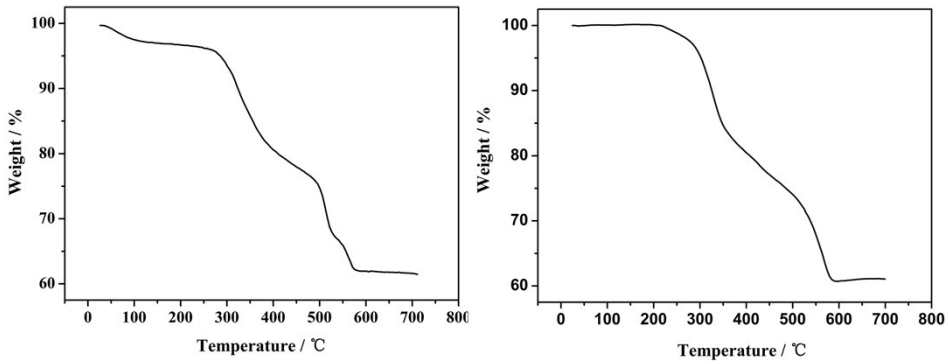

Fig. S3 The TGA curves of **NENU-506** (*left*) and **NENU-507** (*right*) measured in N_2 from room temperature to 700 °C at the heating rate of 5 °C·min^{-1}.

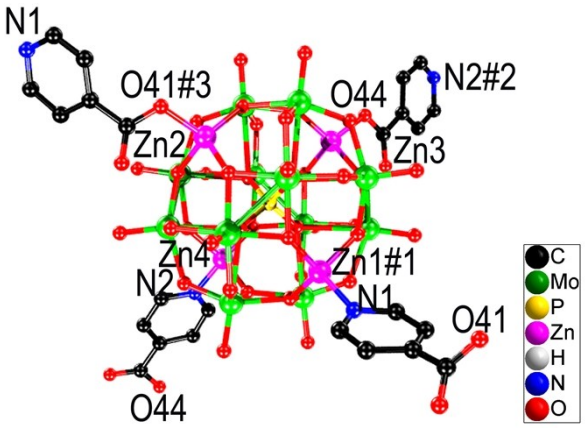

Fig. S4 The coordination environments of Zn (II) centers in **NENU-506**, all hydrogen atoms are omitted for clarity. Symmetry codes: #1 *x*, *y*, *z*; #2 0.5+ *x*, 0.5– *y*, 1 – *z*; #3 *x*, – *y*, 0.5 + *z*.

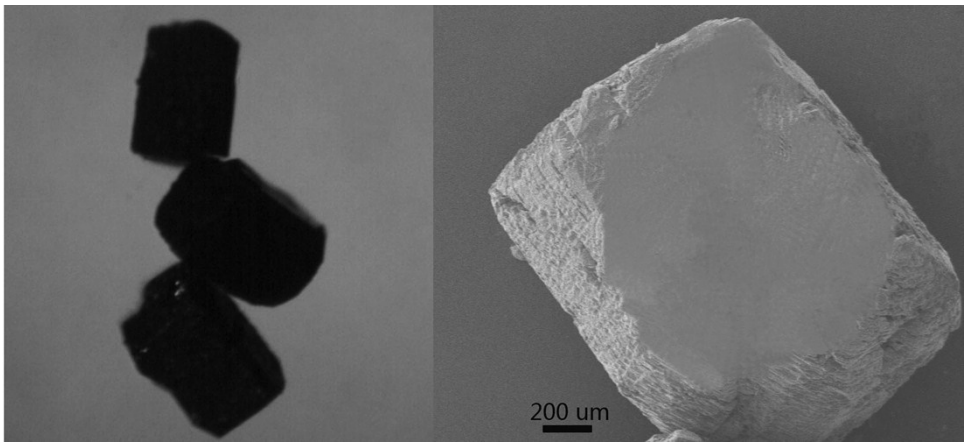

Fig. S5 The images of **NENU-506** under optical microscope (*left*) and under scanning electron microscope (*right*), respectively.

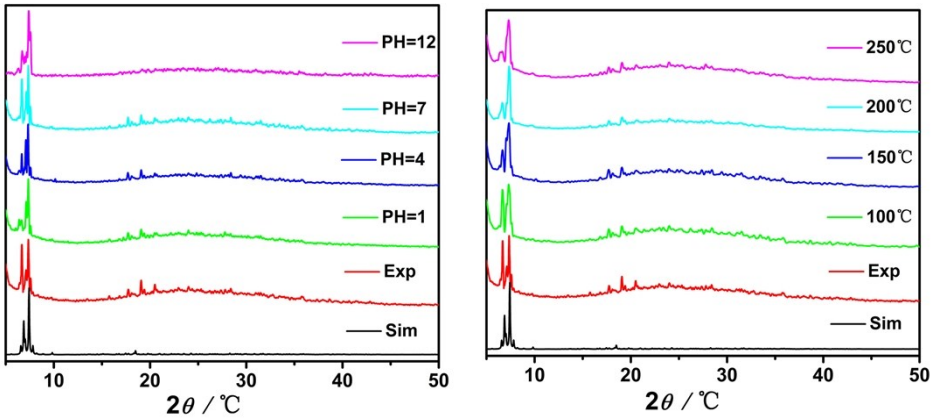

Fig. S6 *Left*: The PXRD patterns of **NENU-506** immersed in water at room temperature for 24 h

at different pH, respectively. *Right*: The PXRD patterns of **NENU-506** after heated at different temperature for 12 h, respectively.

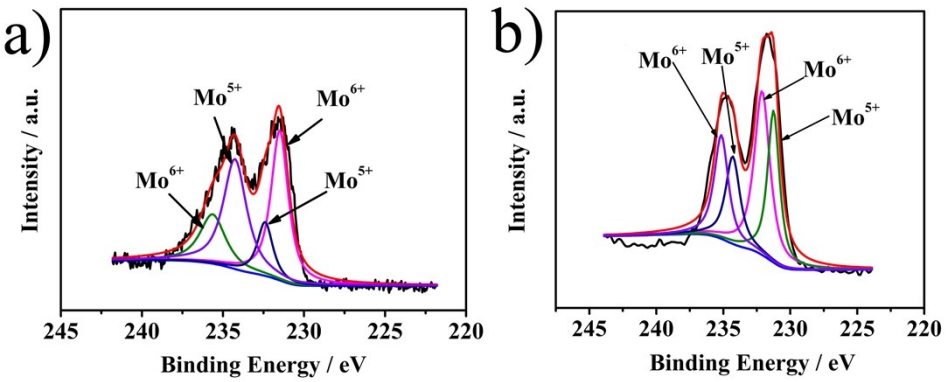

Fig. S7 The XPS analysis of Mo element in **NENU-506** (*left*) and **NENU-507** (*right*), respectively.

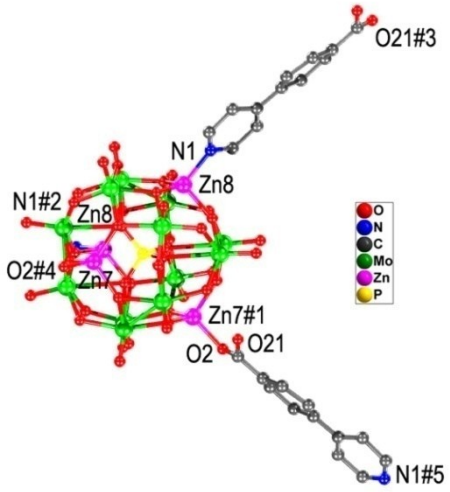

Fig. S8 The coordination environments of Zn (II) centers in **NENU-507**, all hydrogen atoms are omitted for clarity. Symmetry codes: #1 x, y, z; #2 1.25- x, 1.25 – y, 0.25 – z; #3 x, 0.5 + y, –z; #4 1.25- x, 1.25 – y, 0.25 – z, #5 x, –0.5+ y, –z.

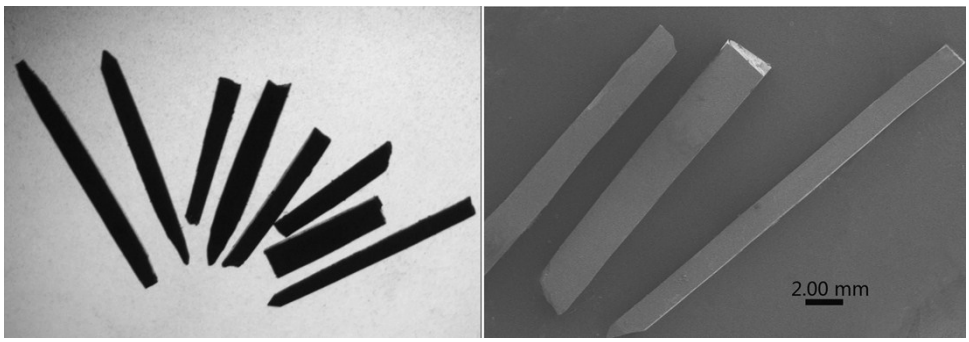

Fig. S9 The images of **NENU-507** under optical microscope (*left*) and under scanning electron microscope (*right*), respectively.

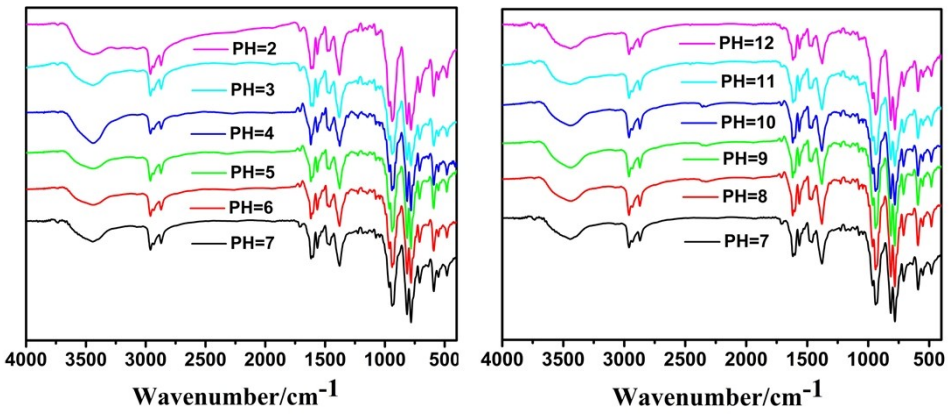

Fig. S10 The IR curves of **NENU-507** immersed in water at different pH for 24 h.

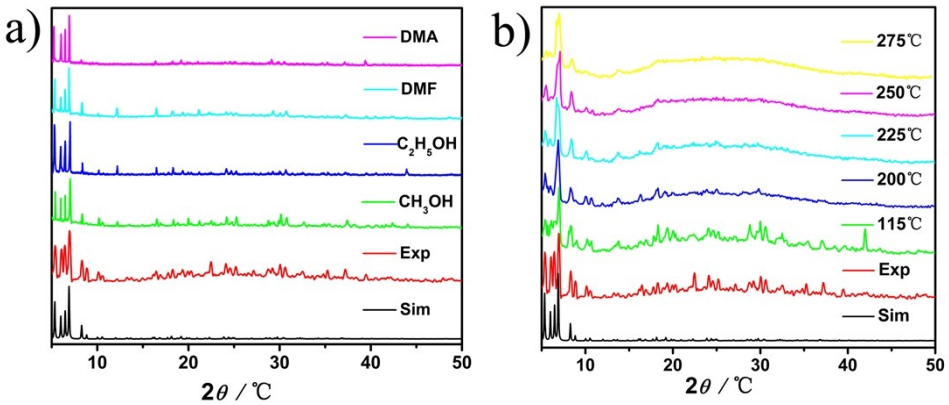

Fig. S11 PXRD patterns of **NENU-507**: (a) soaking in different solvents for 3 days at room temperature and (b) after heating at different temperature for 12 h, respectively.

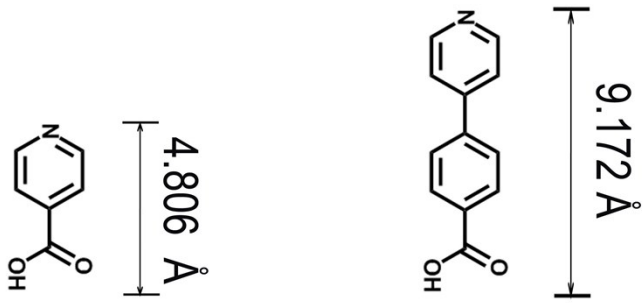

Fig. S12 Illustration of the silimar ligands isonicotinic acid and 4-(pyridin-4-yl) benzoic acid with different coordination length.

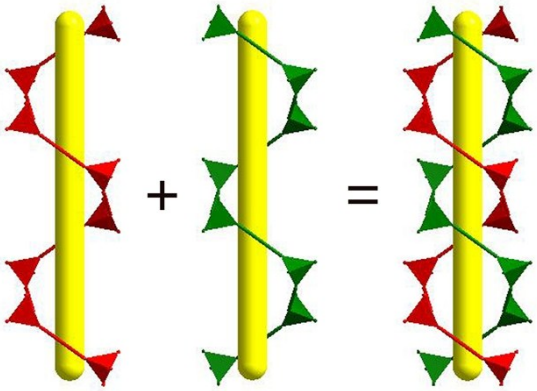

Fig. S13 Ball-and-stick representations of the two handed single helicesin the channel of **NENU-506**.

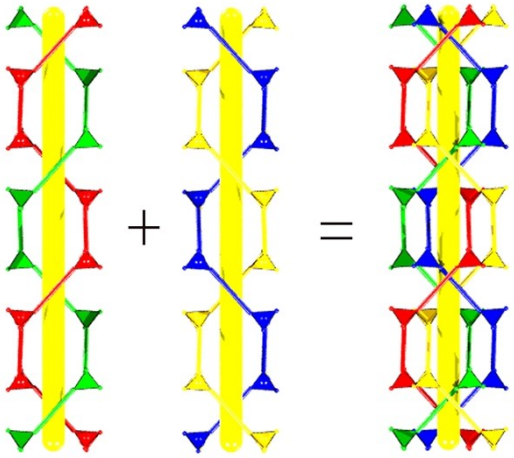

Fig. S14 Ball-and-stick representations of the four handed single helicesin the channel of **NENU-507**.

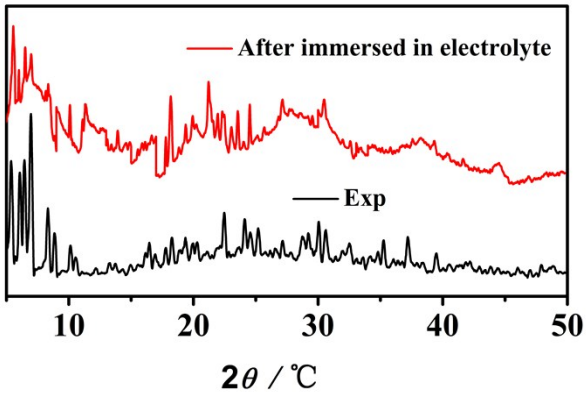

Fig. S15 PXRD patterns of **NENU-507,** the as-synthesized (black), after immersed in electrolyte for 24h at room temperature (red).

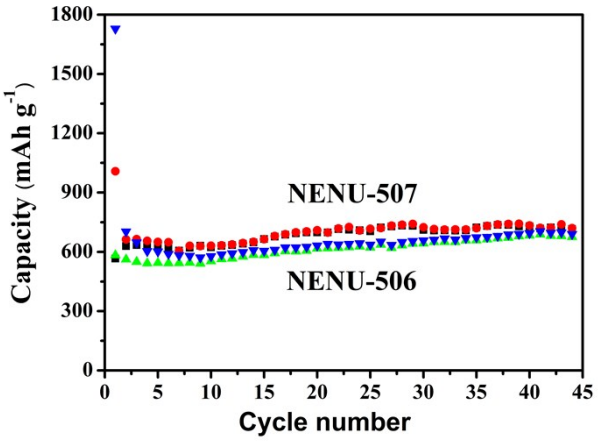

Fig. S16 Cycling performance of **NENU-506** and **NENU-507** at a current density of 100 mA g^{-1}.

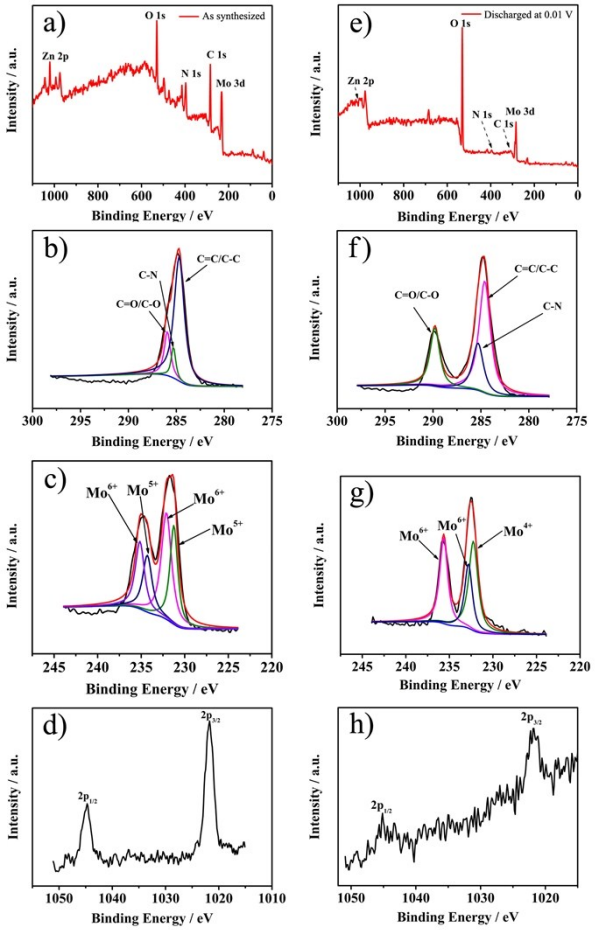

Fig. S17 XPS spectra of **NENU-507** before and after discharged at 0.01 V. (a) - (d): As synthesized powders, (a) Survey scan. (b) C 1s. (c) Mo 3d. (d) Zn 2p; (e) - (f): Discharged at 0.01 V, (e) Survey scan. (f) C 1s. (g) Mo 3d. (h) Zn 2p.

The cells were disassembled in the glove box after discharged at a constant current of 100 mA g^{-1} to 0.01 V. The working electrode was washed with DMC several times before vacuum drying for 12 h at room temperature. Then it will have to be scraped off the Cu foil for XPS tests.

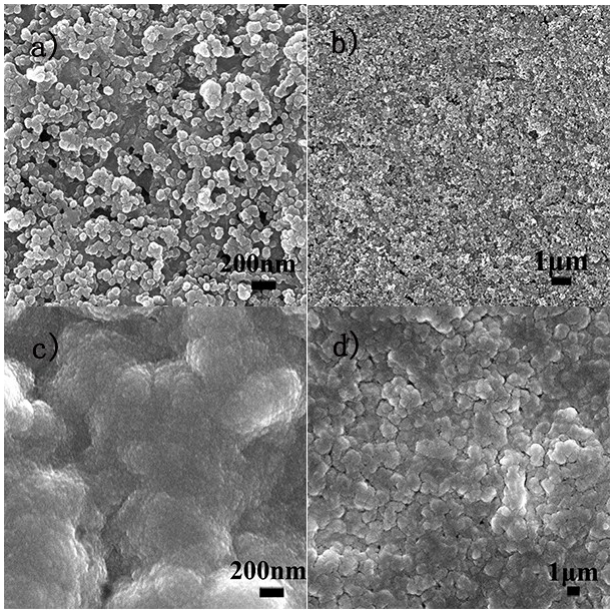

Fig. S18 SEM images of (a) and (b) **NENU-507** electrode (c) and (d) **NENU-507** after 50 cycles performed at a current density of 500 mA g^{-1}.

Electrochemical impedance spectroscopy (EIS) was carried out so as to explore the complex electrochemical processes, applying 5 mV at voltage in the frequency range from 0.01 Hz to 100 kHz. As illustrated in Fig. S19, all of the Nyquist plots consist of one semicircle in the high-frequency range and a linear part in the low frequency range. After 20 cycles, the charge-transfer resistance of **NENU-507** decreased largely, which corresponded to better wetting of the electrodes and improved connectivity.

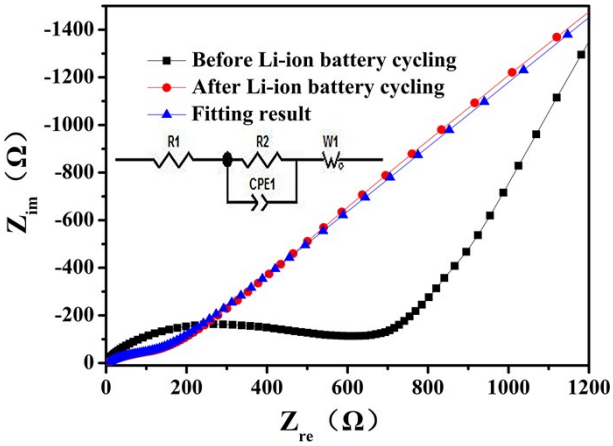

Fig. S19 Nyquist plots of the **NENU-507** as anode material before and after battery cycling. (Inset: Randles equivalent circuit for the NENU-507 electrode/electrolyte interface) R_1 = electronic resistance of the electrodes and electrolyte; R_2 = charge transfer resistance W_o = Warburg impedance related to the diffusion of lithium ions into the bulk electrodes. CPE = constant phase element.

Table S2. Selected bond distances (Å) of **NENU-506**

P(1)-O(7)	1.534	P(1)-O(6)	1.549
P(1)-O(8)	1.541	P(1)-O(5)	1.554
Mo(1)-O(15)	1.699	Mo(7)-O(20)	1.680
Mo(1)-O(36)	1.968	Mo(7)-O(35)	1.886
Mo(1)-O(26)	1.971	Mo(7)-O(36)	1.969
Mo(1)-O(23)	2.002	Mo(7)-O(26)	1.973
Mo(1)-O(32)	2.084	Mo(7)-O(22)	2.037
Mo(2)-O(14)	1.677	Mo(8)-O(11)	1.665
Mo(2)-O(29)	1.957	Mo(8)-O(21)	1.935
Mo(2)-O(30)	1.966	Mo(8)-O(31)	1.947
Mo(2)-O(24)	1.996	Mo(8)-O(4)	1.996
Mo(2)-O(18)	2.094	Mo(8)-O(3)	2.021
Mo(3)-O(12)	1.691	Mo(9)-O(39)	1.685
Mo(3)-O(25)	1.816	Mo(9)-O(2)	1.815
Mo(3)-O(24)	1.835	Mo(9)-O(3)	1.830
Mo(3)-O(33)	2.009	Mo(9)-O(28)	2.016
Mo(3)-O(34)	2.014	Mo(9)-O(1)	2.036
Mo(4)-O(16)	1.708	Mo(10)-O(40)	1.711
Mo(4)-O(27)	1.947	Mo(10)-O(35)	1.946
Mo(4)-O(37)	1.948	Mo(10)-O(30)	1.950
Mo(4)-O(19)	2.039	Mo(10)-O(29)	1.963
Mo(4)-O(32)	2.091	Mo(10)-O(13)	2.014
Mo(5)-O(17)	1.667	Mo(11)-O(9)	1.665
Mo(5)-O(4)	1.950	Mo(11)-O(21)	1.929
Mo(5)-O(31)	1.958	Mo(11)-O(27)	1.962
Mo(5)-O(25)	2.034	Mo(11)-O(37)	1.985
Mo(5)-O(18)	2.062	Mo(11)-O(2)	2.025
Mo(6)-O(38)	1.670	Mo(12)-O(10)	1.676
Mo(6)-O(22)	1.797	Mo(12)-O(19)	1.820
Mo(6)-O(13)	1.841	Mo(12)-O(23)	1.845
Mo(6)-O(1)	2.005	Mo(12)-O(34)	1.989
Mo(6)-O(28)	2.025	Mo(12)-O(33)	2.038
Zn(1)-O(33)	1.902	Zn(3)-O(28)	1.909
Zn(1)-O(36)	1.942	Zn(3)-O(44)	1.945
Zn(1)-O(30)	1.955	Zn(3)-O(29)	1.971
Zn(1)-N(1)	2.003	Zn(3)-O(31)	1.980
Zn(2)-O(41)	1.932	Zn(4)-O(4)	1.921
Zn(2)-O(1)	1.932	Zn(4)-O(37)	1.932
Zn(2)-O(26)	1.963	Zn(4)-O(34)	1.954
Zn(2)-O(27)	1.987	Zn(4)-N(2)	2.018

Table S3. Selected bond distances (Å) of **NENU-507**.

P(1)-O(13)	1.554		
P(1)-O(12)	1.560		
Mo(1)-O(5)	1.946	Mo(4)-O(12)	2.501
Mo(1)-O(1)	1.951	Mo(4)-O(3)	1.948
Mo(1)-O(16)	1.977	Mo(4)-O(11)	2.008
Mo(1)-O(15)	1.659	Mo(4)-O(10)	2.030
Mo(1)-O(17)#1	2.016	Mo(4)-O(22)	1.668
Mo(2)-O(7)#1	1.950	Mo(5)-O(4)	2.027
Mo(2)-O(7)	1.974	Mo(5)-O(6)	2.009
Mo(2)-O(16)#1	1.972	Mo(5)-O(11)	1.829
Mo(2)-O(19)	2.019	Mo(5)-O(9)	1.804
Mo(2)-O(20)	1.683	Mo(5)-O(23)	1.687
Mo(3)-O(5)	1.951	Mo(6)-O(4)	2.000
Mo(3)-O(1)	1.942	Mo(6)-O(6)	2.014
Mo(3)-O(9)	2.013	Mo(6)-O(17)	1.818
Mo(3)-O(14)	1.655	Mo(6)-O(19)	1.820
Mo(3)-O(10)	2.026	Mo(6)-O(18)	1.695
Zn(7)-O(1)	1.981	Zn(8)-O(5)	1.979
Zn(7)-O(4)#1	1.928	Zn(8)-O(7)	1.949
Zn(7)-O(3)	1.961	Zn(8)-O(6)	1.931
Zn(7)-O(2)	1.950	Zn(8)-N(1)	1.976

Table S4. The BVS calculation result of P, Mo and Zn atoms in **NENU-506**

Code	Bond Valence	Code	Bond Valence
P_1	4.867	Mo_1	5.007
Zn_1	2.148	Mo_2	4.986
Zn_2	2.042	Mo_3	5.964
Zn_3	2.057	Mo_4	5.009
Zn_4	2.113	Mo_5	5.559
		Mo_6	6.069
		Mo_7	5.434
		Mo_8	5.452
		Mo_9	4.832
		Mo_{10}	5.294
		Mo_{11}	5.453
		Mo_{12}	5.994

Table S5. The BVS calculation result of P Mo and Zn atoms in **NENU-507.**

Code	Bond Valence	Code	Bond Valence
P_1	4.698	Mo_1	5.328
Zn_7	2.035	Mo_2	5.149
Zn_8	2.108	Mo_3	5.241
		Mo_4	5.115
		Mo_5	5.844
		Mo_6	5.858

Table S6. Comparison of **NENU-507** with other pristine MOFs and POMs based anodes.

Materials	CD ($mA\ g^{-1}$)	CC/DC ($mA\ h\ g^{-1}$)	RC/ Cycles	Ref
NENU-507	**100**	**566/1008**	**640/100**	**This work**
$Co_2(OH)_2(bdc)$	50	1005/1385	650/100	[1]
$SWNTs/Py–SiW_{11}$	0.5 $mA\ cm^{-2}$	586/1569	580/100	[2]
POMOF-1	1.25 C	720/1421	350/500	[3]
$[Cu_2(C_8H_4O_4)_4]_n$	48	194/1492	161/50	[4]
$Mn(tfbdc)(4,4'\text{-}bpy)(H_2O)_2$	50	610/1807	390/50	[5]
$Zn_3(HCOO)_6$	60	693/1344	560/60	[6]
Li/Ni-NTC	100	601/1084	482/80	[7]
$Zn(IM)_{1.5}(abIM)_{0.5}$	100	−/−	190/200	[8]
MOF-177	50	110/425	−/50	[9]

References

[1] L. Gou, L. M. Hao, Y. X. Shi, S. L. Ma, X. Y. Fan, L. Xu, D. L. Li and K. Wang, *J. Solid State Chem.,* 2014, **210**, 121.

[2] D. Ma, L. Y. Liang, W. Chen, H. M. Liu and Y. F. Song, *Adv. Funct. Mater.,* 2013, **23**, 6100.

[3] Y. f. Yue, Y. C. Li, Z. H. Bi, G. Veith, C. Bridges, B. K. Guo, J. H. Chen, D. Mullins, S. Surwade, S. Mahurin, H. J. Liu, M. Parans Paranthaman and S. Dai, *J. Mater. Chem. A*, 2015, **3**, 22989.

[4] R. Senthil Kumar, C. Nithya, S. Gopukumar and M. Anbu Kulandainathan, *Energy Technol.*, 2014, **2**, 921.

[5] Q. Liu, L. Yu, Y. Wang, Y. Ji, J. Horvat, M. L. Cheng, X. Jia and G. Wang, *Inorg. Chem.,* 2013, **52**, 2817.

[6] K. Saravanan, M. Nagarathinam, P. Balaya and J. J. Vittal, *J. Mater. Chem*., 2010, **20**, 8329.

[7] X. Han, F. Yi, T. Sun and J. Sun, *Electrochem. Commun.,* 2012, **25**, 136.

[8] Y. C. Lin, Q. J. Zhang, C. C. Zhao, H. L. Li, C. L. Kong, C. Shen and L. Chen, *Chem. Commun.*, 2015**, 51**, 697.

[9] X. X. Li, F. Y. Cheng, S. N. Zhang and J. Chen, *J. Power Sources*, 2006, **160**, 542.